A Grey Box Method for the Stability Analysis of Multi-Inverter-Fed Power Systems using Bode Diagrams

Grey-Box Stability in Multi-Inverters

Yonggang Li [1], Binyuan Wu [1], Jianwen Li[1*], Yue Wang [2]

[1] School of Electrical and Engineering, North China Electric Power University, Yonghua North Street No. 619, Baoding, China
[2] State Grid Jiangsu electric power company Nantong power supply company, Qingnian Middle Road No. 52, Nantong, China
[*]ljw_ncepu@163.com

Acknowledgments: This work is supported by the Fundamental Research Funds for the Central Universities in China(2023MS109). All Authors express their gratitude here.

A Grey Box Method for the Stability Analysis of Multi-Inverter-Fed Power Systems using Bode Diagrams

Yonggang Li [1], Binyuan Wu [1], Jianwen Li[1*], Yue Wang [2]

[1] School of Electrical and Engineering, North China Electric Power University, Yonghua North Street No. 619, Baoding, China
[2] State Grid Jiangsu electric power company Nantong power supply company, Qingnian Middle Road No. 52, Nantong, China
[*]ljw_ncepu@163.com

Acknowledgments: This work is supported by the Fundamental Research Funds for the Central Universities in China(2023MS109). All Authors express their gratitude here.

Abstract: A multi-inverter-fed power system is susceptible to small-signal instability owing to weak grid influence. Using the impedance-frequency (IF) method to analyse system stability at engineering sites has the following limitations: 1) The internal information of a grid-connected inverter is unknown because of technical confidentiality. Thus, its impedance model should fit in a grey box. 2) The IF method defaults to the subsystem aggregation impedance without right-half-plane (RHP) poles, which may result in incorrect stability analysis. 3) The data used for drawing the IF curve should be calculated per frequency, which is time-consuming. To address these limitations, this study proposes a grey box method for small-signal stability analysis of a multi-inverter-fed power system based on Bode diagrams. First, grey box impedance fitting for a single grid-connected inverter and impedance aggregation for a multi-inverter-fed power system are discussed. Second, the principle of the proposed method is elaborated. Using the Bode diagram, the number of RHP poles of the aggregated impedance and actual number of circles for Nyquist curves are identified. Third, a multi-inverter-fed power system is constructed, and the effectiveness of the proposed method is verified using case analysis and hardware-in-the-loop real-time experiments based on RT-LAB. Finally, the advantages of the proposed method are revealed by comparing it to the IF method.
Keywords: Multi-inverter-fed power system, small-signal stability, grey-box impedance model, impedance-frequency method, Bode diagrams, right-half-plane poles, hardware-in-the-loop experiment

1. Introduction

Stability analysis approaches for a multi-inverter-fed power system should adapt to the replacement of synchronous generators in traditional power systems by clean, inverter-based resources [1]. Unstable accidents, such as those induced by the coupling between grids and grid-connected inverters (GCIs), have been reported [2–4]. The internal parameters, control methods, structure, and other information pertaining to grid-connected inverters at engineering sites are unknown owing to the technical confidentiality restrictions imposed by the equipment supplier. Furthermore, only the impedance model is made available [5]. Hence, analysing the stability of multi-inverter-fed power systems, especially in a grey-box, is a key prerequisite for proposing targeted stability restoration plans [6].

Existing mainstream stability analysis methods include state-space model-based eigenvalue analysis [7–9], and the impedance model-based Nyquist stability criterion [10–12]. Eigenvalue analysis obtains the system mode via eigenvalue decomposition of the state-space matrix and assesses stability by examining whether these modes reside in the right-half-plane (RHP) of the complex frequency domain [7]. This method can use vectors to solve for participation factors [8] and determine parameter-adjustment schemes [9]. While the principles of eigenvalue analysis are well-defined and the analysis process is complete, constructing the state-space matrix of multi-inverter-fed power systems can be challenging owing to poor modification flexibility [10]. The impedance-based stability criterion, which is one of the advantages of the impedance model, is easy to verify and modify. It overcomes the limitations of the state-space model used for eigenvalue analysis. Reference [11] conducted the stability analysis of a single-inverter grid connection by dividing the load and source subsystems, utilising the impedance ratios of the two subsystems and the Nyquist curve. Reference [12] proposed an apparent impedance, extending the criterion presented in [11] to multi-inverter-fed power systems. The impedance-based stability criteria are flexible and widely applicable; however, stability analysis requires accurate determination of the number of RHP poles while the Nyquist curve inflects at (-1, j0) [13].

The impedance-frequency (IF) method, which arises owing to the advantages of impedance-based stability criteria [14–18], equivalently converts the Nyquist curve into real- and imaginary-frequency curves to analyse the stability of multi-inverter-fed power systems intuitively and conveniently. Considering the absence of RHP poles in aggregated impedance, the stability analysis principle of the IF method can be summarised as follows: We determine the frequency at which the imaginary part of the IF curve is zero. If the

impedance corresponding to the value of the real part frequency curve at this frequency is greater than -1, then the Nyquist curve does not surround (-1, j0) and the system is stable; otherwise, the Nyquist curve surrounds (-1, j0) and the system is unstable. Reference [15] was the first to propose an RLC-based IF method. References [16] and [17] use the IF method to reshape quantitative damping and explore frequency coupling. Reference [18] considers the differences in the orders of magnitudes of the parameters and introduces elastic coefficients to improve the IF method. The developments in the impedance-based stability criteria led to the IF method. However, this method has the following limitations while analysing the stability of multi-inverter-fed power systems at engineering sites:

1) The grid-connected inverter is restricted by the technical confidentiality imposed by the equipment supplier. Because the internal information is unknown, the impedance model cannot be established directly.

2) Prior to applying the IF method, the default aggregated impedance has zero RHP poles. Thus, it can only determine whether the Nyquist curve surrounds (-1, j0).

3) The data used for drawing the IF curve must be solved for every frequency. The method has limited applicability owing to its long computational time for wideband and high-order systems.

To solve the above problems for accurate, intuitive, fast, and convenient stability analysis of multi-inverter-fed power systems at engineering sites, this study proposes a grey-box analysis method using Bode diagrams. The contributions of this study are as follows:

1) Considering the confidentiality of proprietary data concerning grid-connected inverters at engineering sites, the grey-box impedance fitting of the grid-connected inverter was performed.

2) Using Bode diagrams, this method can determine the number of RHP poles and circles around the Nyquist curve of the aggregated impedance of each subsystem, ensuring accurate and intuitive stability analysis.

3) Based on the extensive deployment scenarios of Bode diagrams, the proposed method reduces the barriers for engineering and technical personnel, shortens the time required for wideband and high-order system analysis, and ensures a fast and convenient stability analysis.

The remainder of the paper is organised as follows: Section 2 introduces the process of grey-box impedance fitting in for a single grid-connected inverter and impedance aggregation for a multi-inverter-fed power system. Section 3 discusses the principles of the proposed method and impedance-based stability criteria and determines the number of RHP poles and Nyquist circles. Section 4 validates the proposed method using case establishment, analysis, and hardware-in-loop (HIL) real-time simulation experiments. Section 5 reveals the advantages of the proposed method by comparing it to the IF method. Section 6 concludes the study.

2. Grey-box impedance fitting and aggregation

2.1. Grey-box impedance fitting for a grid-connected inverter

Figure 1 shows the topology of an LCL grid-connected inverter [19]. A control block diagram and its equivalent admittance transfer function are presented in the Appendix. This grid-connected inverter is based on the proportional integral (PI) control with d-q-axis decoupling in a rotating coordinate system. This regulates the grid-connected current and suppresses the LCL filter resonance via active damping feedback. In Fig. 1, U_{dc} denotes the DC-side voltage; the LCL filter comprises inductance L_1 on the grid-connected inverter side and L_2 on the grid side and a filtering capacitor C; Z_g and U_g are the equivalent impedance and voltage of the power grid, respectively; I_C, I, and U represent the branch current of the filtering capacitor and grid-connected inverter and voltage at the grid-connected inverter grid-connection point, respectively; PWM and PLL represent pulse width modulation and phase-locked loop, respectively.

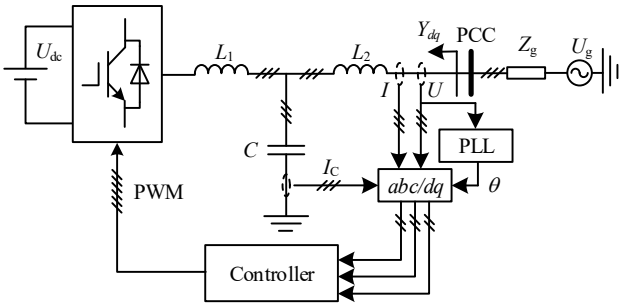

Fig. 1. *Topology of an LCL grid-connected inverter*

The impedance transfer function can be obtained using the internal information of the grid-connected inverter. This type of impedance modelling method is called white-box modelling [20], and its results are expressed as follows:

$$Z(s)=\frac{\beta_b s^b+\beta_{b-1}s^{b-1}+\cdots+\beta_1 s+\beta_0}{\alpha_a s^a+\alpha_{a-1}s^{a-1}+\cdots+\alpha_1 s+\alpha_0}, \quad (1)$$

where α_h (h=1, 2, …, a) and a are the coefficient and highest degree of the non-zero denominator polynomial, respectively; β_h (h = 1, 2, …, b) is the coefficient of molecular polynomial with the highest degree b. J = max{a, b} denotes the order of transfer functions.

The equivalent impedance of a single grid-connected inverter must be obtained using a vector fitting (VF) algorithm [21] based on the discrete frequency response data. This method is called the grey-box method [6, 20, 22], which is implemented as follows:

1) Acquisition of discrete frequency-response data: This type of data is provided by equipment suppliers or measured via disturbance injection [23, 24]. Figure 2 shows the principle of this measurement. The disturbance injection device is connected between the grid-connected inverter and grid series voltage injection and parallel current injection modes [25]. After traversing the grid-connected inverter, the injected disturbance generates a frequency response received by an analyser. The discrete frequency-response data were calculated using the

following equation:

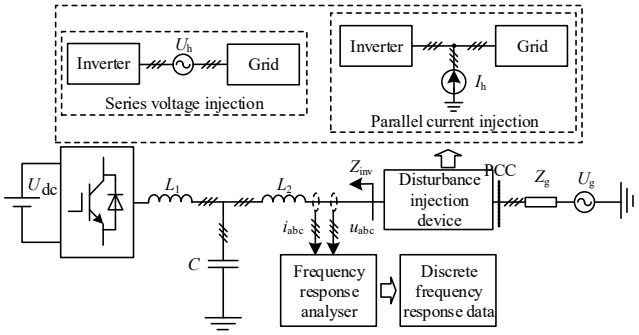

Fig. 2. *Principle of measuring the frequency response data*

$$Z_f = \frac{U_f}{I_f}, \tag{2}$$

where Z_f is the impedance of the grid-connected inverter at frequency f; U_f and I_f are the voltage and current components at frequency f obtained from the fast Fourier transform of the grid-connected inverter port voltages u_{abc} and i_{abc}, respectively.

2) VF calculation: Based on the discrete frequency response data, the equivalent impedance continuous transfer function of the grid-connected inverter can be obtained using VF, as shown in Eq. (3). Reference [26] discusses the principle of the VF algorithm.

$$f(s) \cong \sum_{k=1}^{M_s} \frac{c_k}{s-a_k} + \sum_{k=1}^{M_f} \left(\frac{c_{k1}}{s-a_{k1}} + \frac{c_{k2}}{s-a_{k2}}\right) + d + se, \tag{3}$$

Here, $s = j\omega$ with j being the imaginary unit; a_k is the real-number pole; c_k is the corresponding residue; a_{k1} and a_{k2} are the conjugate complex poles and c_{k1} and c_{k2} are the corresponding conjugate complex residues; d and e are constant terms and first-order real-number coefficients, respectively. When $m > n$ and $e \neq 0$, we have $N = M_s + 2M_f + 1$. When $m \leq n$ and $e = 0$, we have $N = M_s + 2M_f$.

Equations (1) and (3) are interconvertible forms of the transfer functions.

2.2. Impedance aggregation of a multi-inverter-fed power system

Figure 3 shows the simplified topology and equivalent circuit of the multi-inverter-fed power system containing m grid-connected inverters (GCIs). #i denotes the partitioning point of the i-th subsystem, and $Z_{line}i$ is the equivalent impedance of the i-th grid-connected inverter line, where $i \in [1, m]$.

A multi-inverter-fed power system can be divided into source and load subsystems at each grid-connected inverter connection point (#1–#m) or point of common coupling (PCC) (#m+1). The source subsystem is equivalent to a Norton circuit with a current source I_S and the equivalent admittance Y_S connected in parallel. The load subsystem is equivalent to a Thevenin circuit with a voltage source U_L and an equivalent impedance Z_L connected in series. When grid-connected inverters are selected as dividing nodes, one of the inverters serves as the source subsystem, while the remaining components of the system are consolidated into a load subsystem using series and parallel connections. When selecting the PCC as a dividing node, the grid-connected inverters and their connecting lines are parallelly aggregated to form the source subsystem. Furthermore, the grid impedance of the system constitutes the load subsystem. Equation (4) evaluates the aggregated impedance of subsystems with different partition points.

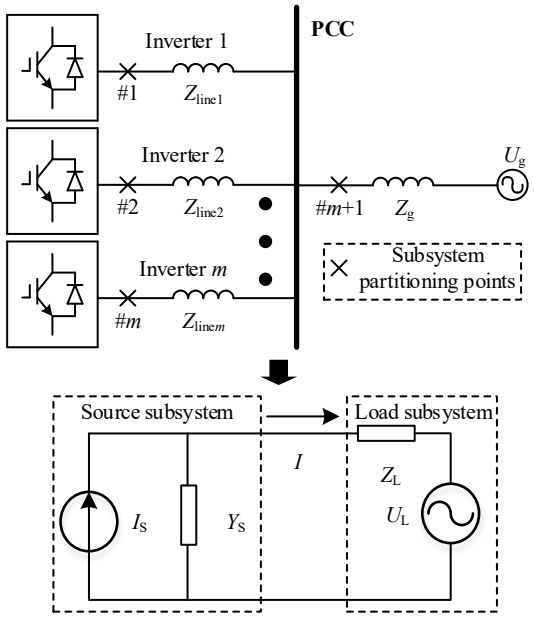

Fig. 3. *Simplified topology and its equivalent circuit for a multi-inverter-fed power system*

$$\begin{cases} Y_S = Y_{GCIi} \\ Z_L = Z_g // Z_{linei} // \bigcap_{j=1, j\neq i}^{m} (Z_{GCIj} + Z_{linej}) \end{cases} \quad \#i, i \in [1, m],$$

$$\begin{cases} Y_S = \dfrac{1}{\bigcap_{j=1}^{m} (Z_{GCIj} + Z_{linej})} \\ Z_L = Z_g \end{cases} \quad \#m+1, \tag{4}$$

Here, $\bigcap_{j=1,j\neq i}^{m} A_j = A_1 // \ldots A_{i-1} // A_{i+1} \ldots // A_m$, // is the parallel calculation operator, and Y_{GCIi} and Z_{GCIi} are the equivalent admittance and impedance of the i-th grid-connected inverter, respectively.

3. Stability analysis using Bode diagrams

3.1. Review of the principles of impedance-based stability criteria

At the partition node shown in Fig. 3, the grid-connected current I of a single or all the inverters is determined as follows:

$$I = (1 + L_m)^{-1} (I_S - U_L Y_S), \tag{5}$$

where $L_m = Z_L Y_S$.

RHP poles of I are evaluated as follows:

$$
\begin{aligned}
P(I) &= P\left(I_S - U_L Y_S\right) + Z\left(1 + L_m\right) \\
&= P\left(1 + L_m\right) + N_{(0,j0)}\left(1 + L_m\right) \\
&= P\left(L_m\right) + N_{(-1,j0)}\left(L_m\right) \\
&= P\left(Z_L\right) + P\left(Y_S\right) + N_{(-1,j0)}\left(L_m\right),
\end{aligned} \tag{6}
$$

where Z(•) and P(•) represent the numbers of RHP zeros and poles, respectively; $N_{(0,\ j0)}(\bullet)$ and $N_{(-1,\ j0)}(\bullet)$ are the total number of turns of the Nyquist curve around the points (0, j0) and (-1, j0), respectively. For $N > 0$ and $N < 0$, the curve revolves clockwise and counterclockwise, respectively.

The impedance-based stability criterion states that a stable grid-connected current I for a single inverter has zero RHP poles. Equation (6) indicates that the number of RHP poles of I is jointly determined using those of the subsystem aggregation impedance Z_L and admittance Y_s and the number of turns of the Nyquist curve of L_m around (-1, j0).

Although the IF method is intuitive and convenient, it assumes that the aggregated impedance of a multi-inverter-fed power system has zero RHP poles. However, this assumption is not always satisfied. Therefore, the application of this method at engineering sites is likely to cause errors. To address this problem, this study investigates the equivalent conversion of the IF method based on the impedance-based stability criterion. Based on Eq. (6), the stability analysis of the multi-inverter-fed power system was performed using Bode diagrams. The following sections discuss the principles of this method.

3.2. Determination of the number of RHP poles

The Bode diagrams of Z_L and Y_s were plotted based on the impedance fitting and aggregation results. According to Reference [27], each amplitude peak in the impedance or admittance Bode diagrams corresponds to a pole. If the phase angle corresponding to the peak frequency exceeds the range of [-90º, 90º], the pole is located at RHP. Consequently, the values of $P(Z_L)$ and $P(Y_S)$ can be determined.

Because most software packages directly plot the Bode diagram for positive frequencies, the default frequency is set to be greater than zero, and negative frequencies are neglected. This simplification does not affect the validity of the principal explanation or the final analysis results. Based on the properties of conjugate complex pole pairs, the amplitude peak with phase angles exceeding the range of [-90º, 90º] and not exceeding 180º or -180º in the Bode diagram should be considered pole pairs with a count of two.

3.3. Determination of the number of Nyquist circles

The Nyquist curve of the transfer function L_m corresponds to the Bode diagram as follows:

1) The unit circle on the Nyquist plane of L_m corresponds to the 0-dB line on the Bode diagram, with the exterior and interior of the circle corresponding to $G(\omega) > 0$ dB and $G(\omega) < 0$ dB, respectively.

2) The negative real axis on the Nyquist plane of L_m corresponds to the phase angle of -180° on the Bode diagram.

The Nyquist curve of L_m revolves around the point (-1, j0) in the anticlockwise direction for one cycle and intersects the negative real axis from the top to the bottom. Consequently, the transfer function phase angle increases with frequency, flipping the phase-angle frequency curve by 180° in the corresponding Bode diagram. If the Nyquist curve of L_m revolves around (-1, j0) in the clockwise direction for one cycle, it must intersect the negative real axis from the bottom to the top. Consequently, the transfer function phase angle decreases with frequency, folding the phase frequency curve at -180° in the corresponding Bode diagram.

The Bode diagram of L_m is drawn using the impedance fitting and product calculation results. The amplitude and phase angle of L_m at frequency f_i were recorded as $M_a(f_i)$ and $P_h(f_i)$, respectively. The following definitions describe the relationship between the Nyquist curve and Bode diagram:

1) **Key frequency point(s).** These are the frequency points f_i that satisfy $M_a(f_i) = 0$ in the amplitude diagram.

2) **Even statistical region.** When the total number of key frequency points is even, the interval between the regions is defined by the corresponding frequencies of each pair of adjacent key frequency points. In this region, $M_a(f_i) > 0$.

3) **Odd statistical region.** When the total number of key frequency points is odd, an interval is created between the minimum key frequency point and imaginary axis. The remaining key frequency points sequentially form several even statistical regions. A single key frequency point corresponds to a single odd statistical region and zero even statistical regions.

4) **Positive crossing.** In the phase angle diagram, the phase angle increases with frequency and crosses the 180º line before flipping downwards. The flipping point is the positive-crossing frequency point.

5) **Negative crossing.** In the phase angle diagram, the phase angle decreases gradually and crosses the -180º line before folding upwards. The turning point is the negative-crossing frequency point.

Figure 4 illustrates the customisation of this study based on the aforementioned definitions.

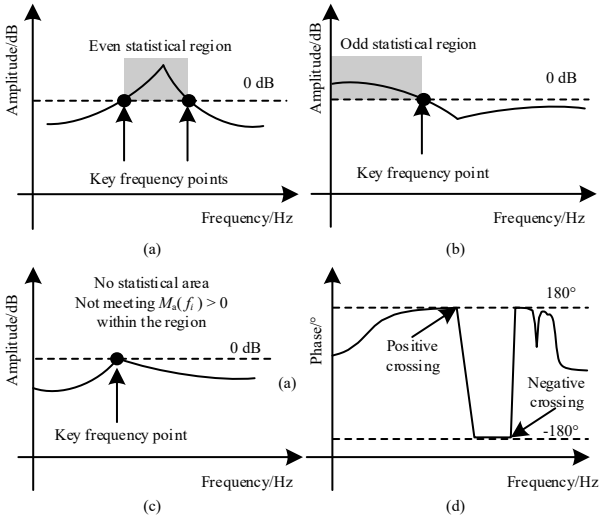

Fig. 4. *Customised schematic description*

N_+ and N_- were respectively recorded as the number of positive and negative crossing frequency points within the statistical region comprising odd and even regions. Beyond the statistical region, we have $N_+ = N_- = 0$. At the frequency origin $f_0 = 0$, we have $N_0 = -1$ for an odd statistical region when the phase angle of the neighbouring frequency point $f_\delta = f_0 + \delta$ (δ is a very small positive integer) on the right-hand side of f_0 is within [0º, 180º]. If the phase angle is within [-180º, 0º], then $N_0 = 1$. Furthermore, $N_0 = 0$ in the absence of odd statistical regions.

When ω varies from -∞ to ∞, the number of circles around the point (-1, j0) in the Nyquist curve of L_m can be equivalently determined based on the Bode diagram of L_m as follows:

$$N_{(-1,j0)}\left(L_m\right) = 2\left(N_- - N_+\right) - N_0. \qquad (7)$$

Let $n = P(Z_L) + P(Y_S)$ and $N = N_{(-1,\,j0)}(L_m)$. When $n-N = 0$, the grid-connected current I of the inverter has zero RHP poles, and the system remains stable based on Eq. (6). When $n-N \neq 0$, I contains RHP poles, which cause system instability.

4. Case analysis and validation

4.1. Basic parameters of the system

A multi-inverter-fed power system was constructed based on the topology in Fig. 2 [27]. The equivalent resistance and inductance of the line were 10 μ Ω /km and 10 μH/km, respectively. The system comprised three (m = 3) LCL grid-connected inverters based on the same control parameters shown in Table 1 and method shown in Fig. 1. The lengths of the lines connecting the three grid-connected inverters to the PCC bus were 1, 2, and 3 km.

Table 1. *Parameters of an LCL grid-connected inverter*

Parameters	Values
DC side voltage U_{dc}/V	1150
Grid-connected voltage U_g/V	575
Grid fundamental frequency f_1/Hz	50
Switching frequency f_r/kHz	10
Inverter side inductance L_1/mH	0.5
Filter capacitor C/μF	50
Grid side inductance L_2/mH	0.2
Proportional coefficient of PLL k_{ppll}	0.7
Integration coefficient of PLL k_{ipll}	3.2
Proportional coefficient of PI controller k_p	1.2
Integrated coefficient of PI controller k_i	65
Active damping coefficient k_c	0.6

Based on the stability analysis in the case study section of [27], two sets of unstable and stable cases were established to verify the accuracy of the method. Case 1: The system is unstable, and the length of the grid-side line is 6 km; Case 2: The system is stable, and the length of the grid-side line is 1 km.

4.2. Case analysis

First, the grey box was fitted to the admittance of a single grid-connected inverter. The frequency band to be analysed was in the range of 100–5000 Hz, and the admittance discrete response data of the grid-connected inverter within the analysed frequency band were obtained via series voltage injection. VF was used for the grey-box fitting of admittance. Figure 5 shows the discrete admittance data points and fitting curve Bode diagram.

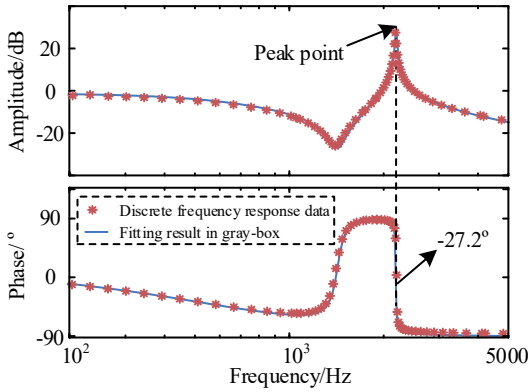

Fig. 5. *Bode diagram of admittance discrete data and fitting curve for single grid-connected inverter.*

The discrete frequency response data coincide with the grey box fitting results, indicating that the admittance of a single grid-connected inverter can be accurately obtained from the grey box, which is consistent with the findings of [27]. Furthermore, the admittance Bode diagram of a single grid-connected inverter shows a peak point with a corresponding phase angle of -27.2º. Hence, a single grid-connected inverter has a complex frequency-domain left-half-plane pole with zero RHP poles. This is consistent with the result that a single grid-connected inverter can maintain stability when connected to an ideal grid.

Subsequently, the number of RHP poles in the load of each partition node or source subsystem was calculated for the two cases. The impedance of the load subsystem was plotted at four partition points, as shown in Fig. 6(a) (Case 1) and Fig. 6(b) (Case 2). When the grid-connected inverters (#1/#2/#3) were used as partitioning points, the source subsystem transformed into a single grid-connected inverter in either case. Figure 5 shows the admittance Bode diagram. When PCC (#4) was used as a

partitioning point, the source subsystem comprised three grid-connected inverters with parallel connecting lines in either case. The length of the grid-side line was different in both cases. Figure 6(c) shows the admittance Bode diagram.

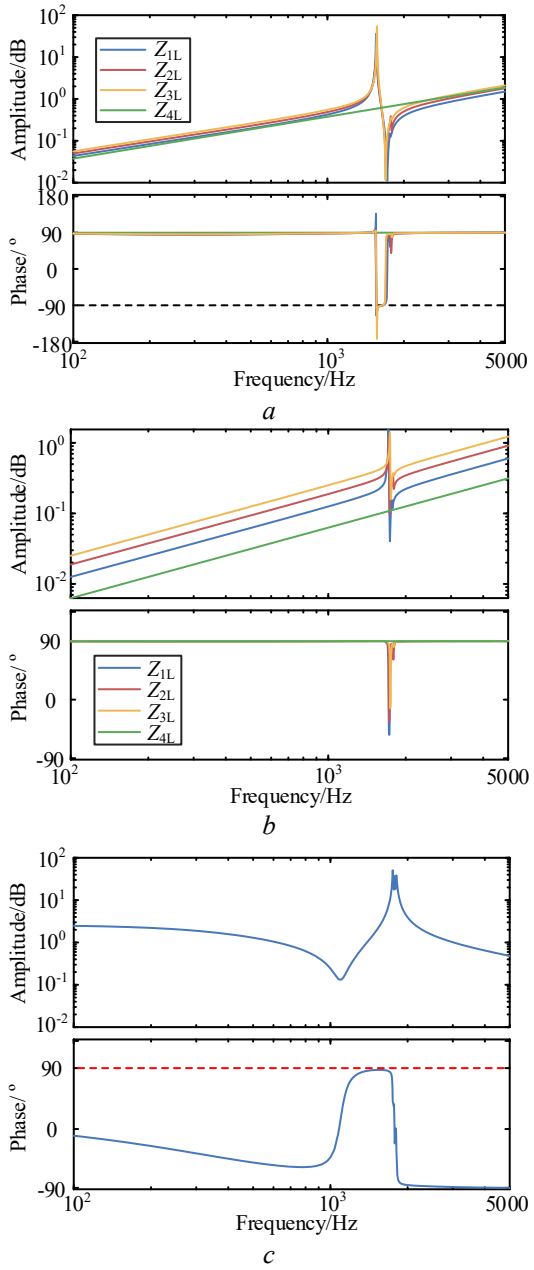

Fig. 6. *Equivalent impedance or admittance of the subsystems. Equivalent impedance of the load subsystem in* ***(a)*** *Case 1 and* ***(b)*** *Case 2.* ***(c)*** *Equivalent admittance Y_{4S} of the source subsystem when dividing the nodes using PCC.*

1) RHP pole counting for the load subsystem: In Case 1 of Fig. 6(a), the equivalent impedances (Z_{1L}, Z_{2L}, and Z_{3L}) of the load subsystem were within the range of [-90º, 90º] when the grid-connection points (#1/#2/#3) were selected for each inverter. Additionally, the corresponding phase angles of the peak frequency points in the Bode diagram were not equal to 180º or -180º. Therefore, Z_{1L}, Z_{2L}, and Z_{3L} contained an RHP conjugate pole pair, i.e., $P(Z_{1L}) = P(Z_{2L}) = P(Z_{3L}) = 2$.

In Case 2 of Fig. 6(b), the phase angles corresponding to the peak frequency points of Z_{1L}, Z_{2L}, and Z_{3L} Bode plots were within the range of [-90º, 90º]. Hence, Z_{1L}, Z_{2L}, and Z_{3L} had zero RHP poles, i.e., $P(Z_{1L}) = P(Z_{2L}) = P(Z_{3L}) = 0$.

The equivalent impedance Z_{4L} of the load subsystem corresponded to the grid impedance when the PCC (#4) was selected as the partitioning node in either case. Additionally, the phase angle corresponding to the peak frequency point of the impedance Bode diagram amplitude was within the range of [-90º, 90º]. Hence, Z_{4L} had zero RHP poles and maintained passivity such that $P(Z_{4L}) = 0$ in both cases.

2) RHP pole counting for source subsystem: The source subsystem was a single grid-connected inverter when the grid-connected points (#1, #2, and #3) were selected for each inverter in either case. The analysis in Fig. 5 indicates that the single grid-connected inverter has zero RHP poles, i.e., $P(Y_{1S}) = P(Y_{2S}) = P(Y_{3S}) = P(Y_{inv}) = 0$.

When PCC (#4) was selected as the partitioning point, the source subsystem comprised three grid-connected inverters and their parallel connecting lines. In both cases, Y_{4S} remained constant, whereas the length of the grid-side line varied. Figure 6(c) shows that the phase angle corresponding to the peak frequency point of the Y_{4S} Bode plot amplitude is within the range of [-90º, 90º]. Hence, Y_{4S} had zero RHP poles, i.e., $P(Y_{4S}) = 0$ in both cases.

The number of circles in the Nyquist curve of L_m around (-1, j0) were equivalently counted using the Bode diagram. Figures 7 and 8 show the Bode diagrams of L_m for each partition node in Cases 1 and 2, respectively.

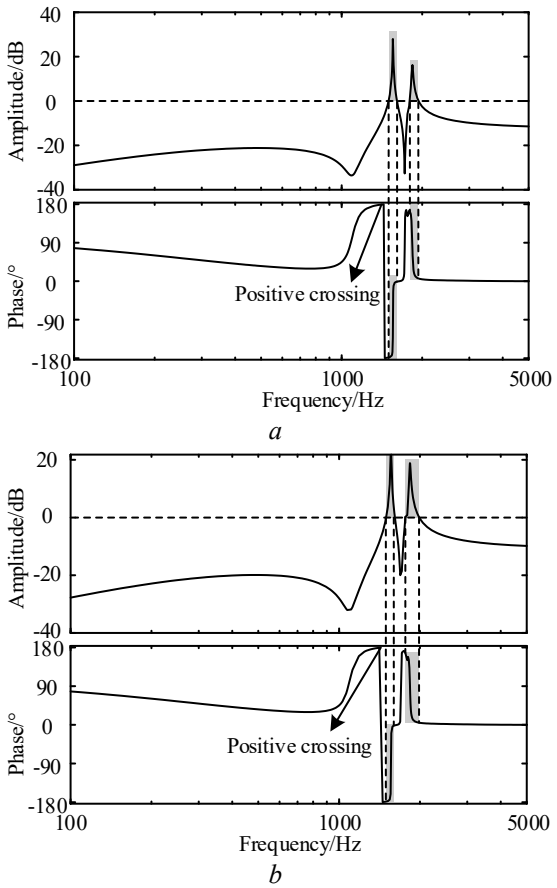

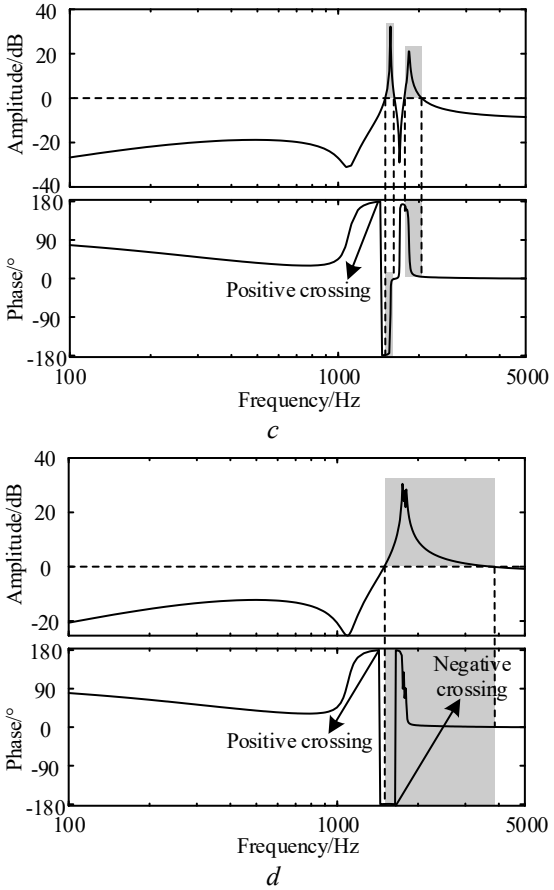

Fig. 7. *Bode diagrams of L_m for each division node in Case 1.* ***(a)*** *#1.* ***(b)*** *#2.* ***(c)*** *#3.* ***(d)*** *#4.*

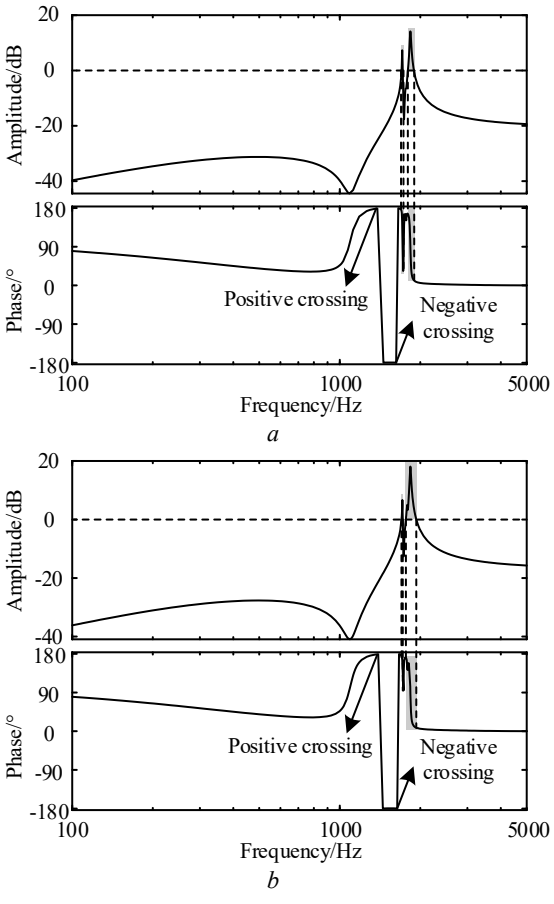

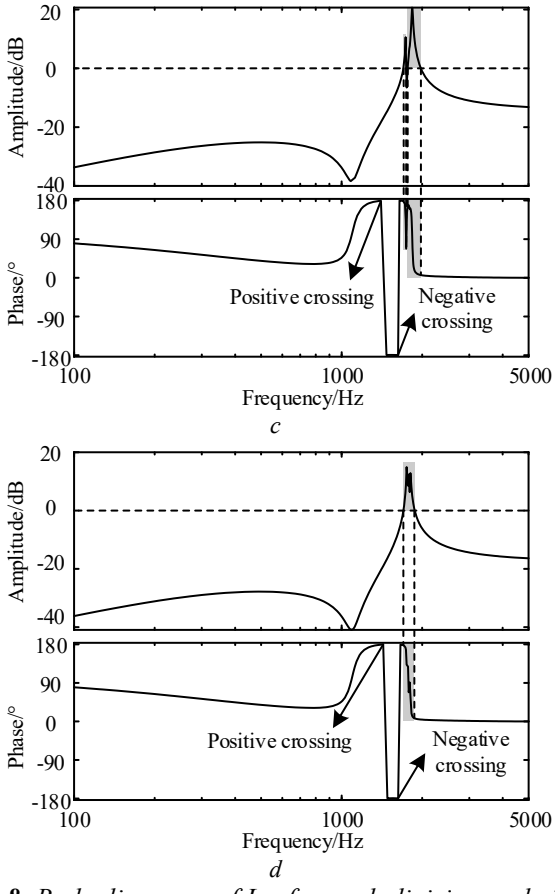

Fig. 8. *Bode diagrams of L_m for each division node in Case 2.* ***(a)*** *#1.* ***(b)*** *#2.* ***(c)*** *#3.* ***(d)*** *#4.*

Figs. 7(a)–(c) show that in Case 1, the Bode diagram of L_m has four key frequency points and one positive intersection for the partitioning nodes #1, #2, and #3, with two even and zero odd statistical regions (N_0 = 0) owing to the even number of key frequency points. Because the intersection does not lie within any statistical region, we have $N_- = N_+ = 0$. Figure 7 (d) shows that the Bode diagram of L_m has two key frequency points corresponding to the positive and negative intersections for the partition node #4, with one even and zero odd statistical region (N_0 = 0) owing to the even number of key frequency points. In contrast to #1, #2, and #3, the positive and negative intersections are in the exterior and interior of the statistical area, respectively. Consequently, $N_- = 1$ and $N_+ = 0$.

Figs. 8 (a)–(c) show that in Case 2, the Bode diagram of L_m has four key frequency points corresponding to one positive and one negative intersection for the partition nodes #1, #2, and #3, with two even and zero odd statistical regions (N_0 = 0) owing to the even number of key frequency points. Neither the positive nor the negative intersections are within any statistical region; hence, $N_- = N_+ = 0$. The Bode diagram of L_m has only two key frequency points for the partition node #4; therefore, there are one even and zero odd statistical regions (N_0 = 0).

Tables 2(a) and (b) represent the stability analysis data for Cases 1 and 2, respectively. Equation (6) was used to calculate the number of RHP poles for the grid-connected current of each partition node, yielding the stability analysis results shown in Table 2.

Table 2. Stability analysis data and results

(a) Case 1

node	$P(Z_{iL})$	$P(Y_{iS})$	$N_{(-1,\,j0)}(L_m)$	$P(I)$	Conclusion
#1	2	0	0	2	Unstable
#2	2	0	0	2	Unstable
#3	2	0	0	2	Unstable
#4	0	0	2	2	Unstable

(b) Case 2

node	$P(Z_{iL})$	$P(Y_{iS})$	$N_{(-1,\,j0)}(L_m)$	$P(I)$	Conclusion
#1	0	0	0	0	Stable
#2	0	0	0	0	Stable
#3	0	0	0	0	Stable
#4	0	0	0	0	Stable

The results and stability analysis conclusions shown in Table 2 are consistent with [27], thereby validating the proposed method.

Table 2 shows that the three inverters have different lengths of the grid-connected lines; however, the system stability analysis data and results for #1, #2, and #3 are similar. Therefore, #1 and #4 were selected as the partitioning nodes to demonstrate the validity and advantages of the proposed method.

4.3. HIL real-time simulation verification

We selected #1 and #4 as typical partition nodes and used an HIL real-time simulation platform, shown in Fig. 9, to perform grid connection experiments on the given system.

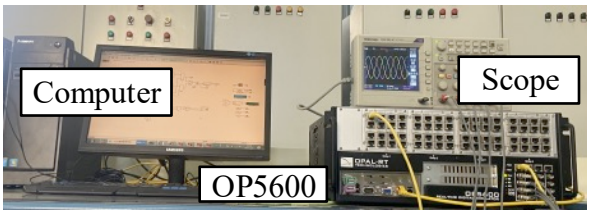

Fig. 9. *HIL real-time simulation platform*

The computer processor of the experimental platform was a 2.5 GHz Intel Core i5. The grid-connected inverter of each node was controlled using an OP5600 real-time digital simulator. RT-LAB software was used to construct the multi-inverter-fed power system and perform disturbance injection. MATLAB 2021a was used to calculate VF and acquire the corresponding transfer function.

The duration of the entire experiment was 1 min, comprising two stages of 30 s each. The first stage was the Case 1 system, wherein three inverters were connected and the grid-side line was 6 km long. The second stage was the Case 2 system wherein three inverters were connected and the grid-side line was 1 km long. Figure 10 shows the two sets of typical waveforms selected for illustration and the grid-connected current of a single inverter at point #1. Figure 11 shows the total grid-connected currents of the three inverters.

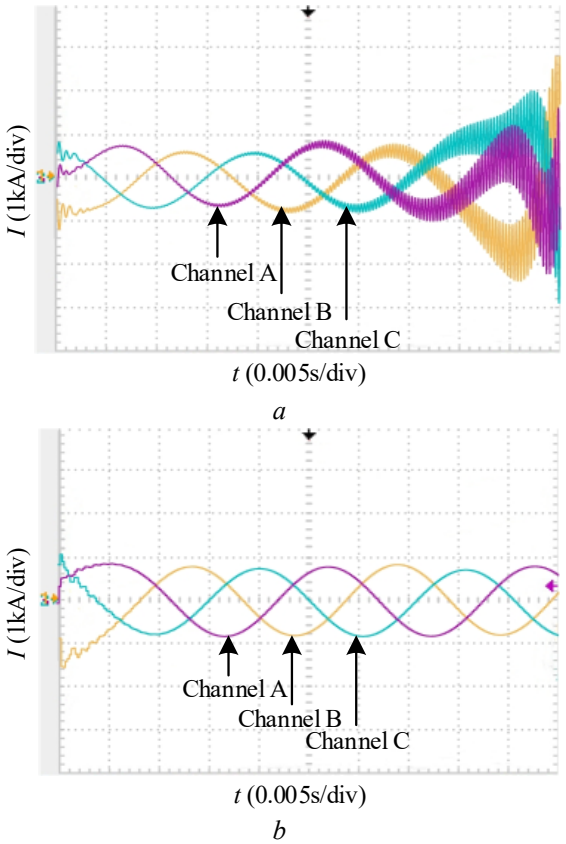

Fig. 10. *Grid-connected current waveform of a single inverter.* ***(a)*** *Case 1 and* ***(b)*** *Case 2.*

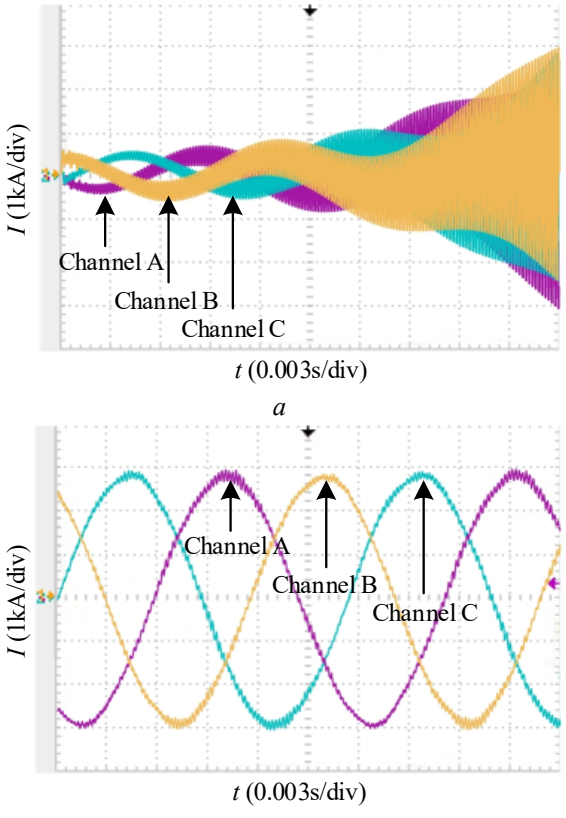

Fig. 11. *Total grid-connected current waveform at #4.* ***(a)*** *Case 1 and* ***(b)*** *Case 2*

Figures 10(a) and 11(a) show that the grid-

connected current of a single inverter and total grid-connected current of inverters diverge for Case 1, corresponding to the unstable multi-inverter-fed power system. Figures 10(b) and 11(b) show that the grid-connected current of a single inverter and total grid-connected current of the inverters are restored to a uniform sinusoidal waveform for Case 2, corresponding to the stable multi-inverter-fed power system.

The comparison of the results shown in Figs. 10 and 11 with the experimental results in [27] indicates that our experimental outcomes are consistent with those in [27], thus validating our experiments. By comparing the stability analysis results obtained using the method presented in Section 4.2, the proposed multi-inverter-fed power system is unstable in Case 1 and stable in Case 2, which is consistent with the experimental results. Therefore, the proposed method is valid.

5. Method comparison and discussion

This section describes the limitations of the IF method to compare and validate the advantages of the proposed method. Case 1 is selected as a typical system, and its stability is analysed using the IF method. MATLAB 2021a was used for the analyses and drawing the Bode diagram on the same computer.

Nodes #1 and #4 were considered typical nodes, and the IF method was used to analyse the system in Case 1, as described in Section 4.1. Figures 12(a) and (b) show the IF curves of L_m of the system.

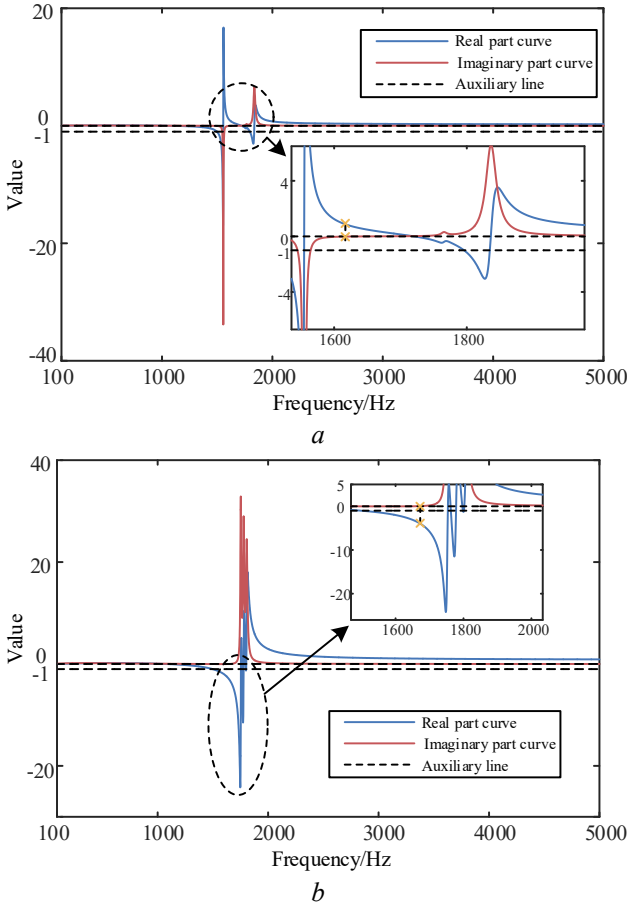

Fig. 12. *IF curve of L_m at* ***(a)*** *#1 and* ***(b)*** *#4 for Case 1*

From Fig. 12(a), the frequency at the intersection of the imaginary part frequency curve and zero value line was found to be 1647 Hz. At this frequency, the value of the real part frequency curve is 1.43, which is greater than -1. According to the stability analysis principle of the IF method, the Nyquist curve does not surround (-1, j0) in the absence of RHP poles in the aggregated impedance. Therefore, the grid-connected current of the first inverter remains stable. However, Fig. 10 (a) indicates that the HIL real-time simulation experiment for the system in Case 1 resulted in an unstable grid-connected current of the first inverter, contradicting the analysis of the IF method. Based on Table 2(a), the erroneous stability analysis of the IF method can be attributed to the two RHP poles in the aggregated impedance of the load subsystem, and the conditions under which the IF method is applicable are no longer satisfied.

Figure 12(b) shows that the frequency at the intersection of the imaginary part frequency curve and zero value line is 1712 Hz. The value of the real part frequency curve at this frequency is -3.83, which is less than -1. According to the stability analysis principle of the IF method, the Nyquist curve surrounds (-1, j0), and the total current of the three inverters connected to the grid is unstable in the absence of RHP poles in the aggregated impedance. This is consistent with the instability phenomenon observed in Fig. 11(a). However, Figures 12(a) and (b) indicates that the IF method can determine whether the Nyquist curve surrounds (-1, j0), it cannot accurately determine the actual number of circles around the curve. Therefore, the risk of incorrect stability analysis increases.

When the same computer was used to calculate and analyse the system in Case 1, the proposed method required 0.424 s for computation, whereas the IF method required 28.623 s. The proposed method has a shorter calculation duration owing to its implementation of Bode diagrams for calculation and analysis. Owing to the built-in Bode diagram drawing program in MATLAB, the proposed method has few technical barriers, rendering it more suitable for practical engineering applications compared to the IF method.

The above comparison indicates that the aggregated impedance RHP poles and number of Nyquist circles should be considered during the stability analysis of multi-inverter-fed power systems. The proposed method is based on impedance-based stability criteria, inheriting the advantages of the IF method. Compared to the IF method, the proposed method can perform stability analysis more accurately, intuitively, rapidly, and conveniently.

6. Conclusion

The stability analysis of a multi-inverter-fed power system should be accurate, intuitive, fast, and convenient. To this end, we proposed a grey-box analysis method for the stability of a multi-inverter-fed power system based on Bode diagrams. The case analysis, HIL real-time simulation verification, and comparison discussion yield the following conclusions:

1) The stability analysis of a multi-inverter-fed power system must consider the engineering applications of internal information confidentiality in grid-connected

inverters. The impedance of each grid-connected inverter can be fitted to a grey box based on the discrete frequency response data combined with the VF algorithm.

2) The stability analysis of a multi-inverter-fed power system requires the simultaneous calculation of the number of RHP poles with aggregated impedance and that of Nyquist curve circles with the impedance ratio. The proposed method uses Bode diagrams to directly determine these quantities. This method is more accurate and intuitive than the IF method.

3) The proposed stability analysis method requires only an impedance grey box model and Bode diagrams, which is advantageous in minimising the calculation time and application barriers for engineering technicians. This method is faster and more convenient than the IF method.

Future studies will explore the underlying reasons for system instability and determine targeted solutions using the proposed method.

7. References

[1] Shi T, Nayanasiri D, Li Y. Sub-synchronous oscillations in wind farms - an overview study of mechanisms and damping methods. IET Renewable Power Generation. 2020;14(19):3974.

[2] Yang X, Li H, Mei Y, Hu X, Wang Y, Xiao X. Application of adaptive chirp mode decomposition on parameter identification of sub/super-synchronous oscillation signals. IET Generation, Transmission & Distribution. 2022;16(2):385.

[3] Zheng C, Li H. Mitigation of sub-synchronous control interaction in DFIGs using active disturbance rejection control. IET Generation, Transmission & Distribution. 2021;15(20):2915.

[4] Liu P, Wang Z, Wei S, et al. Recent developments of modulation and control for high-power current-source-converters fed electric machine systems. CES Transactions on Electrical Machines and Systems. 2020;4(3):215–226.

[5] Zhu Y, Gu Y, Li Y, Green TC. Participation analysis in impedance models: the grey-box approach for power system stability. IEEE Trans. Power System. 2022;37(1):343–353.

[6] Wang X, Blaabjerg F. Harmonic stability in power Electronic-based power systems: concept, modeling, and analysis. IEEE Transactions on Power Electronics. 2020;10(3):2858–2870.

[7] Wang Y, Wang X, Blaabjerg F, Chen Z. Harmonic instability assessment using state-space modeling and participation analysis in inverter-fed power system. IEEE Trans. Ind. Electron. 2017;64(1):806–816.

[8] Yang D, Wang X. Unified modular state-space modeling of grid-connected voltage-source converters. IEEE Transactions on Power Electronics. 2020;35(09):9700–9715.

[9] Ebrahimzadeh E, Blaabjerg F, Wang X, et al. Bus participation factor analysis for harmonic instability in power electronics based power systems. IEEE Transactions on Power Electronics. 2018;33(12):10341–10351.

[10] Zhang H, Wang X, Harnefors L, Gong H, Hasler J-P, Nee H-P. SISO transfer functions for stability analysis of grid-connected voltage-source converters. IEEE Trans. Ind. Electron. 2019;55(3):2931–2941.

[11] Sun J. Impedance-based stability criterion for grid-connected inverters. IEEE Transactions on Power Electronics. 2011;26(11):3075–3078.

[12] Rygg A, Molinas M. Apparent impedance analysis: A small-signal method for stability analysis of power electronic-based systems. IEEE J. Emerg. Sel. Topics Power Electron. 2017;5(4):1474–1486.

[13] Zhou W, Wang Y, Chen Z. Impedance-decoupled modeling method of multiport transmission network in inverter-fed power plant. IEEE Trans. Ind. Electron. 2020;56(1):611–621.

[14] Zhang Q, Mao M, Ke G, Zhou L, Xie B. Stability problems of PV inverter in weak grid: a review. IET Power Electronics. 2020;13(11):2165–2174.

[15] Liang W, Xiaorong X, Qirong J, et al. Investigation of SSR in practical DFIG-based wind farms connected to a series-compensated power system. IEEE Transactions on Power Systems. 2015;30(5):2772–2779.

[16] Li F, Feng Q, Wang Y, Wang H, Ma M, Zhang X. Quantitative damping reshaping method based on equivalent RLC circuits using an active damper. IET Power Electronics. 2022.

[17] Wang Y, Wang L, Jiang Q. Frequency coupling characteristics of electromagnetic oscillation in grid-connected converters. IET Generation, Transmission & Distribution. 2019;13(19):4339–4346.

[18] Qihui L, Chenwei H, Simin P, et al. Analysis and adjustment method of doubly-fed fan control parameters on subsynchronous oscillation based on impedance elastic sensitivity. Transactions of China Electrotechnical Society. 2022;37(14):3528–3541.

[19] Li P, Wang J, Xiong L, Ma M, Wang Z, Huang S. Robust sub-synchronous damping controller to mitigate SSCI in series-compensated DFIG-based wind park. IET Generation, Transmission & Distribution. 2020;14(9):1762–1769.

[20] Stender M, Wallscheid O, Böcker J. Comparison of grey-box and black-box two-level three-phase inverter models for electrical drives. IEEE Trans. Ind. Electron. 2021;68(9):8646–8656.

[21] Wang Y, Wu X, Li Z, Xiao X, Xie X, Wang Y. Vector-fitting-based quantitative SSCI analysis for series-compensated wind power systems. IET Renewable Power Generation. 2020;14(15):3023–3034.

[22] Amin M, Molinas M. A grey-box method for stability and controller parameter estimation in HVDC-connected wind farms based on nonparametric impedance. IEEE Trans. Ind. Electron. 2019;66(3):1872–1882.

[23] Li M, Nian H, Hu B, Xu Y, Liao Y, Yang J. Design method of multi-sine signal for broadband impedance measurement considering frequency coupling characteristic. IEEE J. Emerg. Sel. Topics Power Electron. 2022;10(1):532–543.

[24] Liu J, Du X, Shi Y, Tai H. Impedance measurement of three-phase inverter in the stationary frame using frequency response analyzer. IEEE Trans. Power Electron. 2020;35(9):9390–9401.

[25] Gong H, Wang X, Yang D. DQ-frame impedance measurement of three-phase converters using time-domain MIMO parametric identification. IEEE Trans. Power Electron. 2021;36(2):2131–2142.

[26] Bakhshizadeh MK, Yoon C, Hjerrild J, Bak CL, Kocewiak ŁH, Blaabjerg F, et al. The application of vector fitting to eigenvalue-based harmonic stability analysis. IEEE J. Emerg. Sel. Topics Power Electron. 2017;5(4):1487–1498.
[27] Zhou H, Torres-Olguin RE, Wang Y. A grey-box hierarchical oscillatory instability source identification method of multi-inverter-fed power systems. IEEE Journal of Emerging and Selected Topics in Power Electronics. 2021;9(3):3095–3113.

8. Appendix

Figure A1 shows the single-LCL grid-connected inverter, which adopts the dq-axis decoupling control. The d- and q-axis control links and control parameters are identical, whereas the control variables have coordinate axes and numerical differences. Figure A1 shows a control block diagram based on the d-axis, where $G_i = k_p + k_i/s$ and $G_{del} = e^{-1.5sT_s}$. The subscript *ref* represents the reference value.

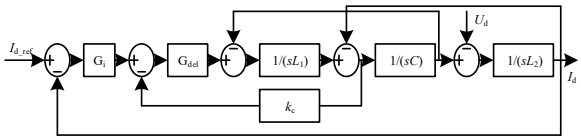

Fig. A1. *Control block diagram of the grid-connected inverter*

Based on the control characteristics and control block diagram, the equivalent admittance Y_{GCI} for a single grid-connected inverter under the dq axis is derived as follows:

$$\boldsymbol{Y}_{GCI} = \begin{bmatrix} Y_{dd} & Y_{dq} \\ Y_{qd} & Y_{qq} \end{bmatrix}, \tag{A1}$$

where $Y_{dq} = Y_{qd} = 0$

$$Y_{dd} = Y_{qq} = \frac{L_1 C s^2 + K_c C G_{del} s + 1}{L_1 L_2 C s^3 + K_c C G_{del} L_2 s^2 + (L_1 + L_2) s + G_i G_{del}}.$$

The control block diagram and equivalent admittance expression provided here should only be used as a reference for readers to reproduce the cases discussed in this study. The relevant information for the actual analysis of the cases is unknown, and the equivalent admittance expression is obtained using the grey-box fitting method introduced in Section 2.